Robust Nonsingular Fixed Time Terminal Sliding Mode Control for Atmospheric Pollution Detection Lidar Scanning Mechanism

KANG Yu · YANG Yuxiao · CHEN Cai · LV Wenjun · ZHAO Yunbo

DOI:
Received: x x 20xx / Revised: x x 20xx

Abstract A robust nonsingular fixed time terminal sliding mode control scheme with a time delay disturbance observer is proposed for atmospheric pollution detection lidar scanning mechanism (APDL-SM) system. Distinguished from the conventional terminal sliding mode control methods, we design a novel fixed-time terminal sliding surface, the convergence time of sliding mode phase of which has a constant upper bound that is designable by adjusting only one parameter. Moreover, in order to overcome the problem of unknown upper bound of lumped uncertainty including model uncertainty, friction effect and external disturbances from the port environment, we propose a time delay disturbance observer to provide an estimation for the system lumped uncertainties. By using the Lyapunov synthesis, the explicit analysis of the convergence time upper bound are performed. Finally, simulation studies are conducted on the APDL-SM system to show the fast convergence rate and strong robustness of the proposed control scheme.

Keywords Fixed time terminal sliding mode, time delay disturbance observer, atmospheric pollution detection lidar, tracking control.

KANG Yu (Corresponding autho)
Department of Automation, University of Science and Technology of China, Hefei 230027, China; Institute of Advanced Technology, University of Science and Technology of China, Hefei 230027, China; State Key Laboratory of Fire Science, University of Science and Technology of China, Hefei 230027, China. Email: kangduyu@ustc.edu.cn
YANG Yuxiao · CHEN Cai · LV Wenjun · ZHAO Yunbo
Department of Automation, University of Science and Technology of China, Hefei 230027, China. Email:yyx531@mail.ustc.edu.cn; cc95@mail.ustc.edu.cn; wlv@ustc.edu.cn; ybzhao@ieee.org

*This research was supported by the National Key Research and Development Project of China under Grant No.2018AAA0100800 and No.2018YFE0106800, National Natural Science Foundation of China under Grant No.61903353, No.61725304 and No.1761673361, Major Science and Technology Project of Anhui Province under Grant No.912198698036, SINOPEC Programmes for Science and Technology Development under Grant No.PE19008-8 and the Fundamental Research Funds for the Central Universities under Grant No.WK2100000013.
◇ *This paper was recommended for publication by Editor .*

1 Introduction

Emissions from ships have been recognized as a significant contributor to the atmospheric environment in coastal areas [1, 2]. Exhaust pollutants such as SO_2, NO_x, particulates and carbonaceous compounds would adversely impact regional air quality, global climate and human health [3–5]. With the rapid development of the maritime industry, the impact of exhaust pollutants from ships on air quality could become more serious in the near future [6, 7]. Atmospheric pollution detection lidar (APDL), which is developed based on the differential absorption laser radar technology, could provide an accurate and fast directional monitoring for atmospheric pollution via a long distance. With the assistance of APDL-SM (i.e., the scanning mechanism of APDL), we can scan the atmospheric area over the ship nozzle and then obtain the thermal map of the exhaust plume. Therefore, in order to track the long-range and small-area targets (i.e., nozzles), the control problem of the azimuth and pitch angle of the APDL-SM arises.

The main difficulty lies in trajectory tracking control with high accuracy and fast response under the issues of high nonlinearity, coupling dynamics, modeling uncertainties, and external disturbances effect. APDL-SM is a typical machinery with two rotational degrees of freedom, the control schemes of which have been investigated intensively, such as adaptive control [8], neural network methods [9, 10], fuzzy logic control [11, 12], and sliding mode control (SMC) [13–16]. Among the aforementioned control methods, SMC has attracted significant attention due to its excellent properties such as strong robustness against parameter changes, model uncertainties, and good rejection of external disturbances [17–20]. However, conventional SMC can only guarantee the asymptotic convergence of states, which implies that high gains are required to obtain the fast convergence and might result in the rapid saturation of actuators [21–24] . To overcome this problem, terminal sliding mode control(TSMC) approach was designed to achieve the finite-time convergence of system dynamics [25–27].

The terminal sliding surface was a nonlinear function of the tracking error and its derivatives, on which the finite-time convergence could be accomplished. Additionally, to eliminate the singularity and accelerate the speed of convergence of TSMC, the nonsingular terminal sliding mode control (NTSMC) and fast nonsingular terminal sliding mode control (FNTSMC) were proposed and achieved a successful applications [28–30]. However, these finite time control methods have a common weakness that the convergence time is affected by the initial state, which means that the control performance of the system might be weakened greatly if the initial state is far away from the sliding surface. Therefore, different from the finite time control methods, the fixed-time control method can guarantee that the convergence time is uniformly bounded by a constant independent of the initial states [31, 32]. However, there are few results in the machinery tracking control by fixed-time control methods. Meanwhile, considering the uncertainty existing in the system, many studies have used the adaptive control method to approximate the uncertainty [33–36]. However, the adaptive control usually needs a long time to stabilize, which might cause the divergence and collapse of the system when applied to the actual APDL-SM system.

As one of the well-known practical nonlinear control strategies for uncertainties, time delay control (TDC) employs a time-delayed estimation (TDE) technique to eliminate the unmodeled dynamics, intractable nonlinearity, and external disturbances [37, 38]. However, in the conventional TDC, the velocity and acceleration signals are calculated by backward differentiator technique, which achieves a lower estimation accuracy due to the differentiating of the measured position signals [39–41]. To deal with this problem, Van *et al.* [42] and Brahmi *et al.* [43] used second-order exact differentiation (SOED) to estimate the velocity and acceleration; however, the SOED can only achieve finite time error convergence, which means that the estimation time of system states rely on the initial states. When the initial states of estimation error are far from the original point, the estimation time increases and consequently the tracking performance deteriorates.

Motivated by the aforementioned discussions and inspired by the attractive attributes of fixed-time control method and TDE, a robust nonsingular fixed time terminal sliding mode (RNFTTSM) control scheme with time delay disturbance observer (TDDO) is proposed for the control of APDL-SM. The contributions are threefold:

(1) We develop a novel fixed time terminal sliding surface (FTTSS) that the convergence time of sliding mode phase has a constant upper bound. The constant upper bound can be designed by adjusting only one parameter.

(2) We propose a new nonsingular fixed time terminal sliding mode (NFTTSM) controller by combining the fixed-time approach law and the proposed FTTSS. The settling time function is upper bounded by a priori value that dose not rely on the system initial state but only on the design parameters. This property implies that the convergence time can be guaranteed in a prescribed manner.

(3) We design a novel robust nonsingular fixed time terminal sliding mode (RNFTTSM) control scheme to improve the robustness of system by introducing a designed TDDO. The TDDO could estimate the lumped uncertainty of the system rapidly and accurately.

The rest of the paper is structured as follows: Section 2 provides the modeling process of APDL-SM and the problem formulation. The notations and preliminaries in this paper are given in Section 3. Section 4 contains the main results, which includes the design of FTTSS , NFTTSM and RNFTTSM control scheme and the corresponding stability analysis. The simulation results to verify the proposed methods are presented in Section 5. Finally, Section 6 concludes this paper.

2 System Modelling and Problem Formulation

In this section, we derive the kinematic model and dynamic model of APDL-SM at first, and then describe the problem studied in this work mathematically.

2.1 APDL-SM Modeling

As a controlled object in control system, APDL-SM can be divided into three parts in the mechanical structure: Chassis (CAS), azimuth rotating part (ARP) , and pitch rotating part

(PRP), which are represented by B_0, B_1, B_2 respectively. The structure diagram of APDL-SM is shown in Figure 1.

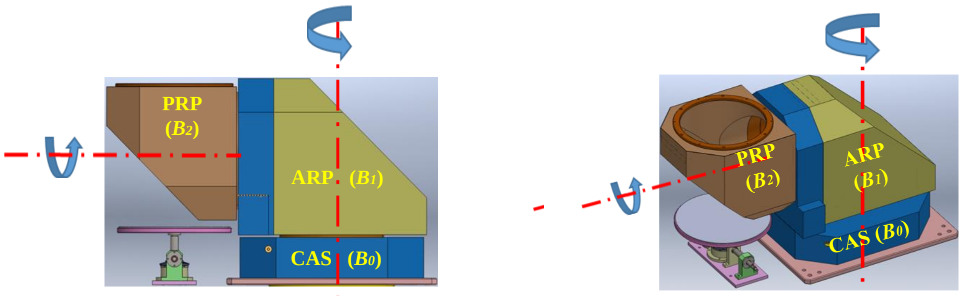

(a) (b)

Figure 1 APDL-SM consists of three parts: CAS (chassis of APDL-SM), ARP (azimuth rotating part), and PRP (pitch rotating part). They are represented by B_0, B_1, B_2 , respectively.

According to the Denavit-Hartenberg Convention, we establish a link frame for APDL-SM, then carry out the kinematic and the dynamic modelling, which are derived as follows.

2.1.1 Kinematics Modeling

Considering the mechanical structure of the APDL-SM, it can be schematically represented from a mechanical viewpoint as a kinematic chain of two rigid bodies (links) connected by two revolute joints, as shown in Figure 2.

[H]

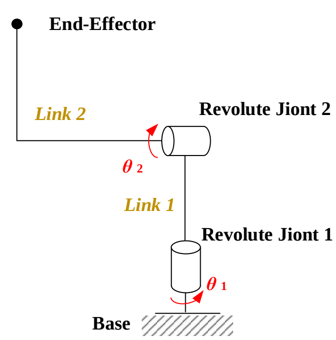

Figure 2 Kinematic Chain

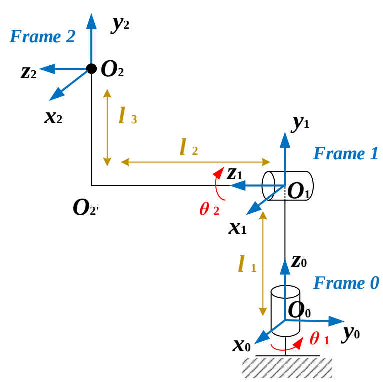

Figure 3 Link Frame

The center of CAS and the central point of the outlet are considered to be the base and end-effector of the kinematic chain, respectively. The joint connecting B_0, and B_1 is considered as $Revolute\,Jiont\,1$. The joint connecting B_1 and B_2 is considered as $Revolute\,Jiont\,2$ which locates at the intersection of the two rotation axes of B_1 and B_2 in the actual mechanism.

According to the Denavit-Hartenberg Convention, the link frame for APDL-SM is established as shown in Figure 3. The origin of $Frame\,0$ coincides with $Revolute\,Jiont\,1$. Analogously, the origin of $Frame\,1$ locates at the intersection between z_0 and z_1. $Frame\,2$ denotes the end-effector frame. $O_{2'}$ denotes the intersection between y_2 and z_1.

On this basis, the Denavit-Hartenberg parameters are specified in Table 1.

Table 1 DH parameters for APDL-SM

Link	a_i	α_i	d_i	θ_i
1	0	$\frac{\pi}{2}$	l_1	θ_1
2	l_3	0	l_2	θ_2

The homogeneous transformation matrices are computed by

$$A_0^1 = A_0^1(\theta_1) = \begin{bmatrix} c_1 & 0 & s_1 & 0 \\ s_1 & 0 & -c_1 & 0 \\ 0 & 1 & 0 & l_1 \\ 0 & 0 & 0 & 1 \end{bmatrix}, \; A_1^2 = A_1^2(\theta_2) = \begin{bmatrix} c_2 & -s_2 & 0 & l_3 c_2 \\ s_2 & c_2 & 0 & l_3 s_2 \\ 0 & 0 & 1 & l_2 \\ 0 & 0 & 0 & 1 \end{bmatrix} \tag{2.1}$$

where c_i denotes $\cos\theta_i$, s_i denotes $\sin\theta_i$, and l_1, l_2, l_3 denote the distances between O_0 and O_1, O_1 and $O_{2'}$, $O_{2'}$ and O_2, respectively.

Then the direct kinematics describing the position and orientation of $Frame$ 2 with respect to $Frame$ 0 is given by

$$T_0^2 = A_0^1 \cdot A_1^2 = \begin{bmatrix} c_1 c_2 & -c_1 s_2 & s_1 & l_3 c_1 c_2 + l_2 s_1 \\ s_1 c_2 & -s_1 s_2 & -c_1 & l_3 s_1 c_2 - l_2 c_1 \\ s_2 & c_2 & 0 & l_3 s_2 + l_1 \\ 0 & 0 & 0 & 1 \end{bmatrix} \tag{2.2}$$

2.1.2 Dynamic Modeling

For dynamic modeling of APDL-SM with n degrees of freedom ($n = 2$), two methods exist: the Euler-Lagrange and the Newton-Euler method. The former approach is energy-based, while the latter analyzes the forces between each of the links in a recursive manner. Considering the non-uniform and asymmetric properties of the mechanical structure of APDL-SM, the potential energy changes over the elevation angle during the scanning movement, so the Newton-Euler method is employed.

For the *augmented Link i* (i.e., *Link i* plus *Joint i*) of the kinematic chain (as shown in Figure 2) and its center of mass C_i, the modeling procedure consists of two recursions: a forward recursion and a backward recursion [44]. Some symbols used in the procedure are given in Table 2.

Table 2 Symbols in Dynamic Modeling for *Link i*

Symbol	**Description**
m_i	mass of *augmented Link* i
$\boldsymbol{I}_i^{\,i}$	inertia tensor of *augmented Link* i with reference to $Frame\, i$
$\boldsymbol{r}_{i-1,i}^{\,i}$	vector from origin of $Frame\,(i-1)$ to origin of $Frame\, i$ with reference to $Frame\, i$
$\boldsymbol{r}_{i,C_i}^{\,i}$	vector from origin of $Frame\, i$ to centre of mass C_i with reference to $Frame\, i$
$\boldsymbol{\omega}_i^{\,i}$	angular velocity of *augmented Link* i with reference to $Frame\, i$
$\dot{\boldsymbol{\omega}}_i^{\,i}$	angular acceleration of *augmented Link* i with reference to $Frame\, i$
$\boldsymbol{v}_i^{\,i}$	linear velocity of origin of $Frame\, i$ with reference to $Frame\, i$
$\dot{\boldsymbol{v}}_i^{\,i}$	linear acceleration of origin of $Frame\, i$ with reference to $Frame\, i$
$\boldsymbol{v}_{C_i}^{\,i}$	linear velocity of centre of mass C_i with reference to $Frame\, i$
$\dot{\boldsymbol{v}}_{C_i}^{\,i}$	linear acceleration of centre of mass C_i with reference to $Frame\, i$
$\boldsymbol{f}_i^{\,i}$	force exerted by $Link\,(i-1)$ on $Link\, i$ with reference to $Frame\, i$
$\boldsymbol{\rho}_i^{\,i}$	moment exerted by $Link\,(i-1)$ on $Link\, i$ with reference to $Frame\, i$
τ_i	the moment resulting at the $RevoluteJoint\, i$

For the forward recursion, link and rotor velocities and accelerations can be computed recursively starting from the velocity and acceleration of the base link by using (2.3), (2.4), (2.5), and (2.6), with known initial conditions $\boldsymbol{\omega}_0^{\,0} = \dot{\boldsymbol{\omega}}_0^{\,0} = [0 \quad 0 \quad 0]^T$,

$$\boldsymbol{\omega}_i^{\,i} = {\boldsymbol{R}_{i-1}^{\,i}}^T (\boldsymbol{\omega}_{i-1}^{\,i-1} + \dot{\theta}_i \boldsymbol{z}_0) \tag{2.3}$$

$$\dot{\boldsymbol{\omega}}_i^{\,i} = {\boldsymbol{R}_{i-1}^{\,i}}^T (\dot{\boldsymbol{\omega}}_{i-1}^{\,i-1} + \ddot{\theta}_i \boldsymbol{z}_0 + \ddot{\theta}_i \boldsymbol{\omega}_{i-1}^{\,i-1} \times \boldsymbol{z}_0) \tag{2.4}$$

$$\dot{\boldsymbol{v}}_i^{\,i} = {\boldsymbol{R}_{i-1}^{\,i}}^T \dot{\boldsymbol{v}}_{i-1}^{\,i-1} + \dot{\boldsymbol{\omega}}_i^i \times \boldsymbol{r}_{i-1,i}^i + \boldsymbol{\omega}_i^i \times (\boldsymbol{\omega}_i^i \times \boldsymbol{r}_{i-1,i}^i) \tag{2.5}$$

$$\dot{\boldsymbol{v}}_{C_i}^i = \dot{\boldsymbol{v}}_i^{\,i} + \dot{\boldsymbol{\omega}}_i^i \times \boldsymbol{r}_{i,C_i}^i + \boldsymbol{\omega}_i^i \times (\boldsymbol{\omega}_i^i \times \boldsymbol{r}_{i,C_i}^i) \tag{2.6}$$

where $\boldsymbol{z}_0$ is the unit vector of the rotational axis of revolute joint, i.e., $\boldsymbol{z}_0 = [0 \quad 0 \quad 1]^T$, $\boldsymbol{R}_{i-1}^i$ is the rotation matrix from $Frame\,(i-1)$ into $Frame\ i$, which can be calculated based Denavit-Hartenberg parameters :

$$\boldsymbol{R}_0^1 = \begin{bmatrix} c_1 & 0 & s_1 \\ s_1 & 0 & -c_1 \\ 0 & 1 & 0 \end{bmatrix}, \quad \boldsymbol{R}_1^2 = \begin{bmatrix} c_2 & -s_2 & 0 \\ s_2 & c_2 & 0 \\ 0 & 0 & 1 \end{bmatrix}$$

Having computed the velocities and accelerations with the forward recursion from the base link to the end-effector, the Newton-Euler equations can be utilized to find the forces and moments acting on each link in a a backward recursion as (2.7) (2.8) (2.9), starting from the force and moment applied to the end-effector, i.e., $\boldsymbol{f}\,^{n+1}_{n+1} = \boldsymbol{\rho}\,^{n+1}_{n+1} = [0 \quad 0 \quad 0]^T$ for $n = 2$.

$$\boldsymbol{f}^i_i = \boldsymbol{R}^{i+1}_i\,\boldsymbol{f}^{i+1}_{i+1} + m_i\,\dot{\boldsymbol{v}}\,^i_{C_i} \tag{2.7}$$

$$\boldsymbol{\rho}^i_i = -\boldsymbol{f}^i_i \times (\boldsymbol{r}^i_{i-1,i} + \boldsymbol{r}^i_{i,C_i}) \,+\, \boldsymbol{R}^{i+1}_i\,\boldsymbol{\rho}^{i+1}_{i+1} \,+\, \boldsymbol{R}\,^{i+1}_i\boldsymbol{f}\,^{i+1}_{i+1} \times \boldsymbol{r}^i_{i,C_i} + I\,^i_i\,\dot{\boldsymbol{\omega}}\,^i_i \,+\, \boldsymbol{\omega}^i_i \times (I^i_i\,\boldsymbol{\omega}^i_i) \tag{2.8}$$

$$\tau_i = {\boldsymbol{\rho}^i_i}^T\,{\boldsymbol{R}^i_{i-1}}^T\,\boldsymbol{z}_0 \tag{2.9}$$

After above calculations, the dynamic model of APDL-SM is established as follows:

$$M(\theta)\,\ddot{\theta} + C(\theta,\dot{\theta})\,\dot{\theta} + G(\theta) = \tau + \tau_d \tag{2.10}$$

in which vectors θ, $\dot{\theta}$, $\ddot{\theta} \in \mathbb{R}^2$, $\theta = [\theta_1, \theta_2]^T$ denotes the joint positions, velocities, and accelerations of APDL-SM, respectively. $M(\theta) \in \mathbb{R}^{2\times 2}$ is a positive definite inertia matrix, $C(\theta,\dot{\theta}) \in \mathbb{R}^{2\times 2}$ is the centripetal Coriolis matrix, $G(\theta) \in \mathbb{R}^2$ is the gravitational vector, $\tau = [\tau_1, \tau_2]^T \in \mathbb{R}^2$ is the joint torque input vector generated by the electrical motors connected to the CAS and ARP of APDL-SM and τ_d is the external disturbance torque vector.

The parameters of APDL-SM are given as follows: $m_1 = 100\,kg$, $m_2 = 46.5\,kg$, $\boldsymbol{r}^1_{0,1} = [0\ ,\ 0.18\ ,\ 0]^T$, $\boldsymbol{r}^2_{1,2} = [0\,,\,0.18\,,\,0.4]^T$, $\boldsymbol{r}\,^1_{1,C_1} = [0\,,\,0.16\,,\,0]^T$, $\boldsymbol{r}\,^2_{2,C_2} = [0\,,\,-0.14\,,\,0]^T$. The inertia tensors of $augmented\,Link\,1$ and $augmented\,Link\,2$ are

$$I\,^1_1 = \begin{bmatrix} 5 & 0 & 0 \\ 0 & 5 & -1.2 \\ 0 & -1.2 & 3.2 \end{bmatrix},\ I\,^2_2 = \begin{bmatrix} 2 & 0 & 0 \\ 0 & 1.3 & 0.2 \\ 0 & 0.2 & 2 \end{bmatrix}$$

Therefore, three nominal matrices in (2.10) are presented as

$$M_0(\theta) = \begin{bmatrix} 9.51\sin^2\theta_2 + 8.74\cos^2\theta_2 + 5 & -0.544\cos\theta_2 \\ -0.544\cos\theta_2 & 2.07 \end{bmatrix} \tag{2.11}$$

$$C_0(\theta,\dot{\theta}) = \begin{bmatrix} 1.55\sin\theta_2\cos\theta_2\cdot\dot{\theta}_2 & 0.54\sin\theta_2\cdot\dot{\theta}_2 \\ -0.77\sin\theta_2 cos\theta_2\cdot\dot{\theta}_1 & 0 \end{bmatrix} \tag{2.12}$$

$$G_0(\theta) = \begin{bmatrix} 0 \\ -18.23\sin\theta_2 \end{bmatrix} \tag{2.13}$$

2.2 Problem Formulation

Considering the modeling uncertainties caused by the asymmetric structural characteristics of APDL-SM, the dynamic equation (2.10) of APDL-SM in the joint space can be expressed as

$$M_0(\theta)\,\ddot{\theta} + C_0(\theta,\dot{\theta})\,\dot{\theta} + G_0(\theta) = \tau + F_d(\theta,\dot{\theta},\ddot{\theta}) \tag{2.14}$$

where $M_0(\theta)$, $C_0(\theta,\dot{\theta})$, $G_0(\theta)$ denote the nominal values, and $F_d(\theta,\dot{\theta},\ddot{\theta}) = \tau_d - \Delta M(\theta)\ddot{\theta} - \Delta C(\theta,\dot{\theta})\dot{\theta} - \Delta G(\theta)$ is the lumped disturbance. $\Delta M(\theta), \Delta C(\theta,\dot{\theta}), \Delta G(\theta)$ stand for the system perturbations, and $\tau_d \in \mathbb{R}^2$ is external disturbances vectors.

The following assumptions are considered for APDL-SM.

Proposition 1 (see [45]) *The inertia matrix $M_0(\theta)$ is positive-definite symmetrical and bounded such that:*

$$\lambda_{min}(M_0)\, I_{2\times 2} \leq M_0(\theta) \leq \lambda_{max}(M_0)\, I_{2\times 2}$$

where $\lambda_{min}(M_0)$ and $\lambda_{max}(M_0)$ are the minimum and maximum eigenvalues of the known inertia matrix $M_0(\theta)$ respectively,and $I_{2\times 2}$ is a 2×2 identity matrix.

Proposition 2 *The matrix $\dot{M}_0(\theta) - 2C_0(\theta, \dot{\theta})$ is skew symmetric.*

Let $\theta_d(t) \in \mathbb{R}^2$ be the desired positon azimuth and pitch of the APDL-SM, then the tracking error can be denoted as $\boldsymbol{e}(t) = [e_1(t),\, e_2(t)]^T \in \mathbb{R}^{2\times 2}$, $\boldsymbol{e}_1(t) = \theta(t) - \theta_d(t)$ and $\boldsymbol{e}_2(t) = \dot{\theta}(t) - \dot{\theta}_d(t)$. The control objective of this paper is to design an nonsingular SMC for APDL-SM, such that the tracking error $\boldsymbol{e}(t)$ can converge to zero within a fixed amount of time, even if APDL-SM is under the effect of unmodeled dynamics, friction vibration and external disturbances:

$$\lim_{t\to t_c} \|\boldsymbol{e}(t)\| = 0 \tag{2.15}$$

where $t_c = t_r + t_s$ is the total settling time of reaching phase and sliding mode phase, and it is available and independent of the initial state.

To solve these problem, let $x_1(t) = \theta(t) \in \mathbb{R}^2$, $x_2(t) = \dot{\theta}(t) \in \mathbb{R}^2$, $x(t) = [x_1(t), x_2(t)]^T \in \mathbb{R}^{2\times 2}$, then APDL-SM dynamic equation (2.14) can be rewritten in the state space form as

$$\begin{aligned} \dot{x}_1(t) &= x_2(t) \\ \dot{x}_2(t) &= f(t,x) + g(t,x)\, u + d(t,x) \end{aligned} \tag{2.16}$$

where $f(t,x) = {M_0}^{-1}(x_1)\big[-C_0(x_1,x_2)\, x_2 - G_0(x_1)\big]$, $g(t,x) = {M_0}^{-1}(x_1)$, and $d(t,x) = {M_0}^{-1}(x_1) \cdot F_d(x_1,x_2,\dot{x}_2)$. $u = \tau$ is the control input. The following assumptions are imposed on system.

Assumption 1 The desired trajectory $\theta_d(t)$ and its first and second-order derivative are known and bounded.

Assumption 2 The lumped uncertainty term $d(t,x)$ is bounded by a known function:

$$\|\, d(t,x)\,\| \leq \Xi(x)\,, \quad \forall(t) \geq 0 \quad \forall(x) \in \mathbb{R}^{2\times 2} \tag{2.17}$$

Assumption 3 The angular position $\theta(t)$, angular velocity $\dot{\theta}(t)$ and angular acceleration $\ddot{\theta}(t)$ are available.

3 Notations and Preliminaries

3.1 Notations

$\mathbb{R}$ denotes the set of real numbers. $\mathbb{R}^+$ denotes the set of positive real numbers. $\mathbb{R}^n$ represents the set of n column vectors. $\mathbb{R}^{n\times n}$ represents the set of $n \times n$ matrices.

As for a vector $a = [a_1, a_2, ..., a_n]^T \in \mathbb{R}^n$, define the absolute value of a as $|a| = \big[|a_1|, |a_2|, ..., |a_n|\big]^T \in \mathbb{R}^n$, where $|\cdot|$ denotes the absolute value of a scalar. The norm of vector a is defined as the Euclidean norm, i.e., $\|a\| = \sqrt{a^T a}$. For the signum function $\mathrm{sgn}(\cdot)$ and a constant γ, define:

$a^\gamma = \left[a_1{}^\gamma,\, a_2{}^\gamma, ...,\, a_n{}^\gamma\right]^T \in \mathbb{R}^n$
$\mathrm{sgn}(a) = \left[\mathrm{sgn}(a_1),\, \mathrm{sgn}(a_2),\, ..., \mathrm{sgn}(a_n)\right]^T \in \mathbb{R}^n,$
$\lfloor a \rceil^\gamma := \left[|a_1|^\gamma \mathrm{sgn}(a_1), .., |a_n|^\gamma \mathrm{sgn}(a_n)\,\right]^T \in \mathbb{R}^n,$
$\lceil a \rfloor^\gamma := \mathrm{diag}\Big(|a_1|^\gamma \mathrm{sgn}(a_1), .., |a_n|^\gamma \mathrm{sgn}(a_n)\Big) \in \mathbb{R}^{n\times n},$
$(a+1)^\gamma := \left[(a_1+1)^\gamma, (a_2+1)^\gamma, ..., (a_n+1)^\gamma\right]^T \in \mathbb{R}^n,$
$\langle a+1 \rangle^\gamma := \mathrm{diag}\Big((|a_1|+1)^\gamma, ..., (|a_n|+1)^\gamma\Big) \in \mathbb{R}^{n\times n}.$

As for a matrix $X \in \mathbb{R}^{m\times n}$, $\|X\|$ represents the Euclidean norm, $X^\sharp$ denotes the column vector of the sum of the absolute values of the elements in each row, i.e.,
$X^\sharp := \Big[\, \sum_{j=1}^n |x_{1j}|,\ \sum_{j=1}^n |x_{2j}|, ...,\ \sum_{j=1}^n |x_{mj}|\, \Big]^T \in \mathbb{R}^n.$

3.2 Preliminaries

Consider the following differential equation system:

$$\dot{x}(t) = F(x(t)),\ x(0) = x_0 \tag{3.1}$$

where $x \in \mathbb{R}^N$, $F(x) : \mathbb{R}_+ \times \mathbb{R}^N \to \mathbb{R}^N$ is a nonlinear function. Suppose that the origin is an equilibrium point of (3.1).

Definition 1 ([46]) The origin of system (3.1) is a finite-time stable equilibrium if the origin is Lyapunov stable and there exists a function $T : \mathbb{R}^N \to \mathbb{R}_+$, called the settling time function, such that for every $x_0 \in \mathbb{R}^N$, the solution $x(t, x_0)$ of system (3.1) is defined on $[0, T(x_0))$, with $x(t, x_0) \in \mathbb{R}^N$ for all $t \in [0, T(x_0))$, and $\lim_{t\to T_{x_0}} x(t, x_0) = 0$.

Definition 2 ([46]) The origin of (3.1) is said to be a fixed-time stable equilibrium point if it is globally finite-time stable with bounded settling time $T(x_0)$, i.e., $\exists\, T_{max} > 0$ such that $T(x_0) < T_{max}$, $\forall x_0 \in \mathbb{R}^N$.

Lemma 1 ([47]) Consider a scalar system

$$\dot{y} = -\alpha\, y^{\frac{m}{n}} - \beta\, y^{\frac{p}{q}},\ y(0) = y_0 \tag{3.2}$$

where $\alpha > 0$, $\beta > 0$, and m, n, p, q are positive odd integers satisfying $m > n$ and $p > q$. Then the equilibrium of (3.2) is fixed-time stable and the settling time T is bounded by

$$T < T_{max} \triangleq \frac{1}{\alpha}\frac{n}{m-n} + \frac{1}{\beta}\frac{q}{q-p} \tag{3.3}$$

4 Control Scheme Design and Stability Analysis

It consists of two parts: NFTTSM controller and the RNFTTSM control scheme, which combines NFTTSM with a time delay distuebance observer (TDDO). They will be introduced in detail respectively as follows.

4.1 FTTSS

First of all, a new fixed time terminal sliding surface (FTTSS) is designed as:

$$\sigma(e) = e_2 + 2\beta \lceil e_1 \rfloor^{\frac{1}{2}} (|e_1| + 1)^{\frac{3}{2}} \tag{4.1}$$

where $\beta = \mathrm{diag}(\beta_1, \beta_2)$ is a positive definite matrix.

Theorem 1 Consider the tracking error dynamic system (2.14) with our proposed FTTSS (4.1) satisfying $\sigma = 0$. Then $e_1 = 0$ and $e_2 = 0$ can be reached in a fixed time t_s, whose upper bound can be estimated as

$$t_s \le T_s = (\beta^{-1})^{\sharp} \tag{4.2}$$

Proof Once a sliding motion is established on the surface $\sigma = 0$, the dynamics of the variable $e_1(t)$ are governed by:

$$\dot{e}_1 = -2\beta \lceil e_1 \rfloor^{\frac{1}{2}} (|e_1| + 1)^{\frac{3}{2}} \tag{4.3}$$

it can be written as

$$-\beta \, dt = \frac{1}{2} \lceil e_1 \rfloor^{-\frac{1}{2}} (|e_1| + 1)^{\frac{1}{2}} \, de_1 \tag{4.4}$$

By solving the differential equation (4.4), the convergence time of the system states on the proposed FTTSS $\sigma = 0$ can be calculated as

$$t_s = \beta^{-1} \lceil e_1 \rfloor^{\frac{1}{2}} (|e_1| + 1)^{-\frac{1}{2}} \tag{4.5}$$

Consider that the upper bound of both elements in the vector $\lceil e_1 \rfloor^{\frac{1}{2}} (|e_1| + 1)^{-\frac{1}{2}}$ is 1, therefore, once the sliding surface is attained, the states e_1, e_2 can reach the origin within a fixed time with the upper bound T_s:

$$t_s \le T_s = (\beta^{-1})^{\sharp} \tag{4.6}$$

where $(\cdot)^{\sharp}$ denotes the column vector of a matrix, which calculates the sum of the absolute values of the elements in each row. ∎

4.2 NFTTSM Controller

Considering the Assumption 3 that the angular position $\theta(t)$ and angular velocity $\dot{\theta}(t)$ are both available, we design a controller for system (2.14) such that the desired trajectory can be reached in fixed time, which means that the total convergence time is independent of initial states.

According to the terminal sliding mode design procedure, the nonsingular fixed time terminal sliding mode controller is designed as

$$u = u_{eq} + u_{re} \tag{4.7}$$

where u_{eq} is used to control nominal component, and u_{re} is introduced to deal with the uncertainty. u_{eq} can be obtained by solving the equation $\dot{\sigma} = 0$ with $d(t, x) = 0$

$$\begin{aligned} u_{eq} = -g^{-1}(t, x) \Big[& f(t, x) + 4\beta \lceil e_1 \rfloor^{\frac{1}{2}} \langle e_1 + 1 \rangle^{\frac{1}{2}} e_2 + \\ & + \mathrm{sat}\Big(\beta \lceil e_1 \rfloor^{-\frac{1}{2}} \langle e_1 + 1 \rangle^{\frac{1}{2}} e_2, \ h \Big) \Big] \end{aligned} \tag{4.8}$$

In (4.8), a saturation function is applied to handle the singularity by limiting the amplitude of singularity term $\lceil e_1 \rfloor^{-\frac{1}{2}}$, and the saturation function can be defined as

$$\operatorname{sat}(x, y) = \begin{cases} x, & \text{if } |x| < y \\ y \cdot \operatorname{sgn}(x), & \text{if } |x| \geq y \end{cases} \tag{4.9}$$

To guarantee the fixed-time convergence to the sliding surface, revisit Lemma 1 and then design the reaching law:

$$\dot{\sigma} = -k_1 \, \sigma^{\frac{p}{q}} - k_2 \, \sigma^{\frac{m}{n}} - \Xi(x)\operatorname{sgn}(\sigma) \tag{4.10}$$

where $k_1 = \operatorname{diag}(k_{11}, \, k_{12})$, $k_2 = \operatorname{diag}(k_{21}, \, k_{22})$ are positive definite matrix, m, n, p, q are positive odd integers satisfying $m > n$ and $p < q$. Therefore, we can obtain u_{re} as

$$u_{re} = -g^{-1}(t, x)\big[k_1 \, \sigma^{\frac{p}{q}} + k_2 \, \sigma^{\frac{m}{n}} + \Xi(x)\operatorname{sgn}(\sigma)\big] \tag{4.11}$$

Theorem 2 Considering the dynamic system (2.16) satisfying Assumption 1, 2 , 3, the sliding mode σ and the tracking errors e_1 and e_2 will converge to the origin within fixed time via the proposed FTTSS (4.1) and NFTTSM controller (4.7) (4.8) (4.11), and the settling time t_c is bounded by

$$t_c \leq T_c = (\beta^{-1} + \frac{n}{m-n} {k_1}^{-1} + \frac{q}{q-p} {k_2}^{-1})^{\sharp} \tag{4.12}$$

Proof Consider the following Lyapunov candidate function as

$$V_1 = \frac{1}{2} \, \sigma^T \sigma \tag{4.13}$$

The time derivative of V_1 can be obtained as $\dot{V}_1 = \sigma^T \dot{\sigma}$, and yields

$$\dot{V}_1 = \sigma^T \Big[f(t, x) + g(t, x) \, u + d(t, x) + 4\beta \lceil e_1 \rfloor^{\frac{1}{2}} \langle e_1 + 1 \rangle^{\frac{1}{2}} e_2 + \beta \lceil e_1 \rfloor^{-\frac{1}{2}} \langle e_1 + 1 \rangle^{\frac{1}{2}} e_2 \Big] \tag{4.14}$$

Substituting the NFTTSM controller (4.7) (4.8) (4.11) into (4.14), we have

$$\begin{aligned} \dot{V}_1 &= -\sigma^T \Big[k_1 \sigma^{\frac{p}{q}} + k_2 \sigma^{\frac{m}{n}} + \Xi(x)\operatorname{sgn}(\sigma) - d(t, x) + \operatorname{sat}(\Gamma, h) - \Gamma \Big] \\ &= -\sigma^T \Big[k_1 \sigma^{\frac{p}{q}} + k_2 \sigma^{\frac{m}{n}} \Big] - \sigma^T \Big[\Xi(x)\operatorname{sgn}(\sigma) - d(t, x) \Big] - \sigma^T \Big[\operatorname{sat}(\Gamma, h) - \Gamma \Big] \\ &\leq -\lambda_{min}(k_1) V^{\frac{p+q}{2q}} - \lambda_{min}(k_2) V^{\frac{m+n}{2n}} - \|\sigma\| \big[\Xi(x) - \|d(t, e)\| \big] - \|\sigma\| \, \big[\|\operatorname{sat}(\Gamma, h)\| - \|\Gamma\| \big] \\ &= -\lambda_{min}(k_1) V^{\frac{p+q}{2q}} - \lambda_{min}(k_2) V^{\frac{m+n}{2n}} - \|\sigma\| \cdot \mu - \|\sigma\| \cdot \nu \end{aligned} \tag{4.15}$$

where $\Gamma = \beta \lceil e_1 \rfloor^{-\frac{1}{2}} \langle e_1 + 1 \rangle^{\frac{1}{2}} e_2$, $\mu = \Xi(x) - \|d(t, x)\|$, $\nu = \|\operatorname{sat}(\Gamma, h)\| - \|\Gamma\|$, $\lambda_{min}(k_i)$ denotes the minimum eigenvalue of the positively definite matrix k_i, therefore, we have

$$-\lambda_{min}(k_1) \, V^{\frac{p+q}{2q}} - \lambda_{min}(k_2) \, V^{\frac{m+n}{2n}} < 0 \tag{4.16}$$

According to (2.17), one has $\mu = \Xi(x) - \|d(t, x)\| > 0$ so that it yields

$$-\|\sigma\| \cdot \mu < 0 \tag{4.17}$$

To confirm the sign of $-\|\sigma\|\cdot\nu$, define the singularity area Ω as the region where inequality $|\Gamma| \geq h$ holds. The following analysis will be divided into two cases.

For the case of $|\Gamma| < h$, on the basis of (4.9), we have $\text{sat}(\Gamma, h) = \Gamma$, which gives rise to $\nu = \|\text{sat}(\Gamma, h)\| - \|\Gamma\| = 0$, thus $-\|\sigma\|\cdot\nu < 0$. Based on the (4.16) and (4.17), it is concluded that $\dot{V}_1 < 0$, so that it is asymptotically stable.

For the case of $|\Gamma| \geq h$, the tracking error $e_1(t)$ can be obtained by $e_1(t) = e_1(0)+\int_0^t e_2(\tau)d\tau$. If $e_2(t) > 0$ holds, $e_1(t)$ will increase monotonically and leave the singularity area Ω. If $e_2(t < 0)$ holds, $e_1(t)$ will decrease monotonically and also leave the singularity area. Both situations prove that the system lies in the singularity region transiently. Therefore, the existence of singularity region does not influence the results of the stability analysis.

According to Lemma 1 and the reaching law in (4.10), system (2.16) reaches the sliding surface within a bounded time, and the bound of convergence time can be estimated by

$$t_r \leq T_r = \left(\frac{n}{m-n}{k_1}^{-1} + \frac{q}{q-p}{k_2}^{-1}\right)^{\sharp} \tag{4.18}$$

When the system reaches the sliding surface $\sigma = 0$, recalling Theorem 1 yields that the state variable $e_1(t)$ can be stabilized within a finite time bounded by

$$t_s \leq T_s = (\beta^{-1})^{\sharp} \tag{4.19}$$

When state variable $e_1(t)$ settles down to the origin, the state variable $e_2(t)$ also converges to zero. Consequently, the convergence time for system (2.16) can be estimated as

$$\begin{aligned} t_c &= t_r + t_s \\ &\leq T_r + T_s = (\beta^{-1} + \frac{n}{m-n}{k_1}^{-1} + \frac{q}{q-p}{k_2}^{-1})^{\sharp} \end{aligned} \tag{4.20}$$

The proof is completed. ∎

Remark 1 In order to guarantee that $\sigma = 0$ lies outside the singularity area Ω, as pointed out in [46], the parameter h in control law (4.8) can be set to satisfy

$$h > \beta\lceil e_{1max}\rfloor^{-\frac{1}{2}}\langle e_{1max}+1\rangle^{\frac{1}{2}} \cdot \left(2\beta\lceil e_{1max}\rfloor^{\frac{1}{2}}(|e_{1max}|+1)^{\frac{3}{2}}\right) \tag{4.21}$$

$$\Longrightarrow h > 2\beta^2 \cdot \left(|e_{1max}|+1\right)^2 \tag{4.22}$$

where $e_{1\max}$ denotes the maximum of $|e_1|$.

Remark 2 In the proposed controller (4.7) (4.8) (4.11), the design procedure is based on the assumption that the upper bound function $\Xi(x)$ of the unknown function $d(t, x)$ can be obtained in advance. However, this approach limits its applications because the exact upper bound function is difficult to obtain beforehand in real application. In order to resolve this limitation, a TDDO will be developed in the next section, and the RNFTTSM control scheme is proposed as a result.

4.3 RNFTTSM

In this section, we propose a robust nonsingular fixed time terminal sliding mode (RNFTTSM) contol scheme based on a time delay disturbance observer (TDDO). Another assumption is made as follows.

Assumption 4 The lumped uncertainty term $d(t,x)$ is continuous over time t, and continuously differentiable with respect to the time variable, and do not vary largely during a small period T_L of time.

According to the assumption above, the lumped uncertainty term $d(t,x)$ can be considered as a continuous function, and thus the following approximation is satisfied based on TDE technique:

$$d(t,x) \cong d(t-T_L,x) \tag{4.23}$$

Consequently, the estimation of the $d(t,e)$ can be obtained, that is,

$$\widehat{d}(t,x) \triangleq d(t-T_L,x) \tag{4.24}$$

where $\widehat{d}(t,x)$ is the estimation of lumped uncertainty $d(t,x)$ at the time t.

Remark 3 In practice, the smallest achievable T_L is the sampling period in digital implementation. A digital control system behaves reasonably close to the continuous system if the sampling rate is faster than 30 times the system bandwidth [48]. Hence, with a T_L smaller than this level, the continuous lumped uncertainty $d(t,e)$ can be estimated by using the TDE.

From the dynamic system (2.16) and (4.24), the TDDO can be obtained as

$$\begin{aligned}\widehat{d}(t,x) &\triangleq d(t-T_L,x)\\ &= \dot{x}_2(t-T_L) - f(t-T_L,x) - \Big(g(t-T_L,x)u\Big) = d_{TDDO}\end{aligned} \tag{4.25}$$

where $f(t-T_L,x) = \Big\{M_0{}^{-1}(x_1)\big[-C_0(x_1,x_2)x_2 - G_0(x_1)\big]\Big\}\Big|_{t-T_L}$ and $g(t-T_L,x) = \big\{M_0{}^{-1}(x_1)\big\}\Big|_{t-T_L}$.

From (4.23), (4.25), the unknown lumped uncertainty function can be described by the proposed TDDO with the observation error δ as

$$d(t,x) = d_{TDDO} + \delta \tag{4.26}$$

where δ is the observation error. Based on the analyses in [[49],[50]], the assumption below is reasonable for a sufficiently small T_L.

Assumption 5 There exist a positive constant $\overline{\delta}$ such that $|\delta| \le \overline{\delta}$, and $\overline{\delta}$ is a known upper bound of TDDO error.

From (4.26), the dynamic system described in (2.16) can be rewritten as

$$\begin{aligned}\dot{x}_1(t) &= x_2(t)\\ \dot{x}_2(t) &= f(t,x) + g(t,x)\,u + d_{TDDO} + \delta\end{aligned} \tag{4.27}$$

For this system, the derivative of the sliding surface σ defined in (4.1) can be rewritten as

$$\begin{aligned}\dot{\sigma} =& f(t,x) + g(t,x)\,u + d_{H\text{-}TDDO} + \delta \\ &+ 4\beta\lceil e_1\rfloor^{\frac{1}{2}}\langle e_1+1\rangle^{\frac{1}{2}}e_2 + \beta\lceil e_1\rfloor^{-\frac{1}{2}}\langle e_1+1\rangle^{\frac{1}{2}}e_2\end{aligned} \tag{4.28}$$

Then the RNFTTSM control scheme is now designed based on TDDO to accommodate unmodeled dynamics, friction vibration and external disturbances.

$$u = u_{eq} + u_{TDDO} + u_{re} \tag{4.29}$$

where u_{eq} is designed as the same as (4.8):

$$\begin{aligned}u_{eq} = -g^{-1}(t,x)\Big[& f(t,x) + 4\beta\lceil e_1\rfloor^{\frac{1}{2}}\langle e_1+1\rangle^{\frac{1}{2}}e_2 + \\ &+ \operatorname{sat}\Big(\beta\lceil e_1\rfloor^{-\frac{1}{2}}\langle e_1+1\rangle^{\frac{1}{2}}e_2,\ h\Big)\Big]\end{aligned} \tag{4.30}$$

The lumped uncertainty compensation term based on TDDO is

$$u_{TDDO} = -g^{-1}(t,x)\ d_{TDDO} \tag{4.31}$$

and u_{re} is designed as

$$u_{re} = -g^{-1}(t,x)\big[k_1\,\sigma^{\frac{p}{q}} + k_2\,\sigma^{\frac{m}{n}} + \overline{\delta}\cdot\operatorname{sgn}(\sigma)\big] \tag{4.32}$$

The parameters in (4.32) have the same definitions in (4.11). And the stability of the system under the proposed RNFTTSM control scheme in (4.31) is demonstrated as follows.

Theorem 3 Considering the APDL-SM dynamic system (4.27) under Assumption 1 to Assumption 5, the sliding mode σ and the tracking errors e_1 and e_2 will converge to the origin within fixed time via the proposed FTTSS (4.1) and RNFTTSM control law (4.29) (4.30) (4.31) (4.32)

Proof Let the Lyapunov candidate function be

$$V_2 = \frac{1}{2}\sigma^T\sigma \tag{4.33}$$

Differentiating V_2 with respect to time and substitute (4.28) into it, we have

$$\begin{aligned}\dot{V}_2 &= \sigma^T\dot{\sigma} \\ &= \sigma^T\Big[f(t,x) + g(t,x)u + (d_{TDDO} + \delta) \\ &\quad + 4\beta\lceil e_1\rfloor^{\frac{1}{2}}\langle e_1+1\rangle^{\frac{1}{2}}e_2 + \beta\lceil e_1\rfloor^{-\frac{1}{2}}\langle e_1+1\rangle^{\frac{1}{2}}e_2\Big]\end{aligned} \tag{4.34}$$

then, substitute the RNFTTSM control law (4.29) to (4.32) into above, it yields

$$\begin{aligned}\dot{V}_2 &= -\sigma^T\big[\operatorname{sat}(\Gamma,h) - \Gamma + k_1\sigma^{\frac{p}{q}} + k_2\sigma^{\frac{m}{n}} + \overline{\delta}\cdot\operatorname{sgn}(\sigma) - \delta\big] \\ &= -\sigma^T\big[k_1\sigma^{\frac{p}{q}} + k_2\sigma^{\frac{m}{n}}\big] - \sigma^T\big[\overline{\delta}\cdot\operatorname{sgn}(\sigma) - \delta\big] - \sigma^T\Big[\operatorname{sat}(\Gamma,h) - \Gamma\Big] \\ &\le -\lambda_{min}(k_1)V^{\frac{p+q}{2q}} - \lambda_{min}(k_2)V^{\frac{m+n}{2n}} - \|\sigma\|\Big[\|\operatorname{sat}(\Gamma,h)\| - \|\Gamma\|\Big] \\ &= -\lambda_{min}(k_1)V^{\frac{p+q}{2q}} - \lambda_{min}(k_2)V^{\frac{m+n}{2n}} - \|\sigma\|\cdot\nu\end{aligned} \tag{4.35}$$

where Γ and ν have the same definations as (4.15).

Based on (4.35) and the proof for Theorem 1, we can verify that the trajectories of (4.1) and the tracking errors e_1 and e_2 will converge to the origin within fixed time without singularity under the control law defined in (4.29) to (4.32). This completes the proof for Theorem 3. ▮

Remark 4 Considering that the proposed control laws (4.11) and (4.32) consist the signum function $\mathrm{sgn}(\cdot)$, the chattering is inevasible in the system. However, the chattering amplitude is related to the upper bound of lumped uncertainty or the upper bound of TDDO error. Therefore, the chattering can be reduced to the acceptable limits due to TDDO and the proposed methods can used in APDL-SM system.

5 Comparative Study and Discussion

To demonstrate the effectiveness of the proposed control schemes, numerical simulations for the azimuth and pitch angle of the APDL-SM to track a given desired trajectory are carried out under the proposed control scheme. Rewrite the dynamic equation of APDL-SM (2.14) as follows:

$$M_0(\theta)\,\ddot{\theta} + C_0(\theta,\dot{\theta})\,\dot{\theta} + G_0(\theta) = \tau + F_d(\theta,\dot{\theta},\ddot{\theta}) \tag{5.1}$$

where the three nominal matrices are presented as

$$M_0(\theta) = \begin{bmatrix} 9.51\sin^2\theta_2 + 8.74\cos^2\theta_2 + 5 & -0.544\cos\theta_2 \\ -0.544\cos\theta_2 & 2.07 \end{bmatrix} \tag{5.2}$$

$$C_0(\theta,\dot{\theta}) = \begin{bmatrix} 1.55\sin\theta_2\cos\theta_2\cdot\dot{\theta}_2 & 0.54\sin\theta_2\cdot\dot{\theta}_2 \\ -0.77\sin\theta_2 cos\theta_2\cdot\dot{\theta}_1 & 0 \end{bmatrix} \tag{5.3}$$

$$G_0(\theta) = \begin{bmatrix} 0 \\ -18.23\sin\theta_2 \end{bmatrix} \tag{5.4}$$

The desierd trajectory for azimuth and pitch angle of APDL-SM are selected as

$$\theta_d = \begin{bmatrix} 1.45 - 1.4e^{-t} + 0.6e^{-4t} \\ 1.25 + e^{-t} - 0.5e^{-4t} \end{bmatrix} \tag{5.5}$$

5.1 Convergence Time of Sliding Mode Phase on FTTSS

Assign the parameter β in FTTSS with $\mathrm{diag}(2,4)$. The initial states of positon tracking error on sliding surface are set $e_1(0) = [3,-1]^T$. The results are shown in Figure 4(a). We can observe that the convergence time for position tracking error of azimuth angle e_{11} and pitch angle e_{12} is less than $0.5s$ and $0.25s$, respectively; therefore, it verified that the convergence time of sliding mode phase has the upper bound β^{-1} presented in Theorem 1.

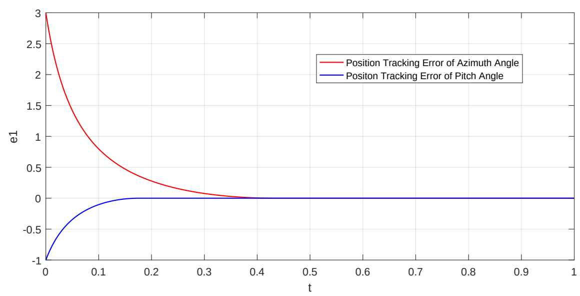

(a) when $\beta = diag(2, 4)$

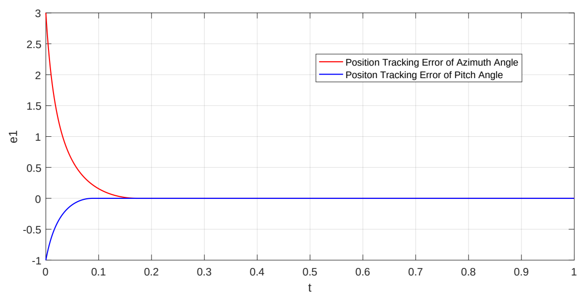

(b) when $\beta = diag(5, 8)$

Figure 4 Convergence time of sliding mode phase

Setting $\beta = \text{diag}(5, 8)$ and then yielding Figure 4(b), the Theorem 1 could be also verified. Therefore, it is clear that the convergence time of the position tracking error on sliding mode phase can be modified optionally by changing the parameter β of our proposed FTTSS.

5.2 Control Performance of the Proposed NFTTSM Controller

The unmodeled dynamics including parametric uncertainties is chosen as 0.2 times the normal dynamics, while the external disturbances follows

$$\tau_d = \begin{bmatrix} 2\,\text{sin}t + 0.5\sin\left(200\,\pi t\right) \\ \cos(2t) + 0.5\sin\left(200\,\pi t\right) \end{bmatrix} \tag{5.6}$$

Five groups of initial states $x(0)^1 = [0.2, 2.1, 0, -0.1]^T$, $x(0)^2 = [0.8, 3, 0.5, 0.5]^T$, $x(0)^3 = [1.2, 0.2, -0.4, 1.4]^T$, $x(0)^4 = [1.5, 1.3, 0.1, 6]^T$, $x(0)^5 = [-0.4, 2.3, -0.2, -3]^T$ are considered, respectively. The parameters of our NFTTSM controller are selected as $k_1 = 0.5, k_2 = 1, m = 5, n = 3, p = 1, q = 9, \beta_1 = \beta_2 = 8$. Under the same settings of controller parameters and external disturbance, the simulation results of ARP and PRP in ADPL-SM with five groups of initial states are shown in Figure 5 and Figure 6.

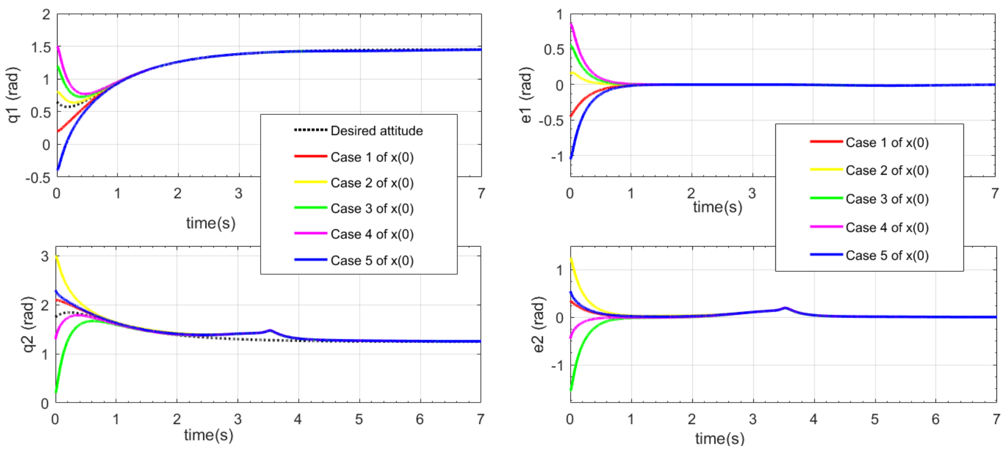

(a) Angle tracking trajectory (b) Angle tracking error

Figure 5 Angle tracking trajectory and tracking error trajectory of ARP and PRP in APDL-SM with five cases of initial states.

Based on the results in Theorem 1 and Theorem 2, the upper bound of the convergence time during reaching phase and sliding mode phase can be calculated by NFTTSM controller parameters as $t_r \leq T_r = 3.75s$ and $t_s \leq T_s = 0.125s$. As a consequence, the total setting time t_c can be estimated as $t_c \leq T_c = T_r + T_s = 3.875s$. Compared with the following practical numerical results, the estimated convergence time is conservative.

Figure 5(a) and Figure 5(b) show the response curves of angle and angular tracking error trajectory with different initial states. It is observed that the proposed NFTTSM controller has fast global convergence speed and the tracking errors decrease to zero promptly. The convergence time under the proposed NFTTSM controller is smaller than $1.5s$, which is much less than the calculated value before. The settling time is independent to the starting points of the states.

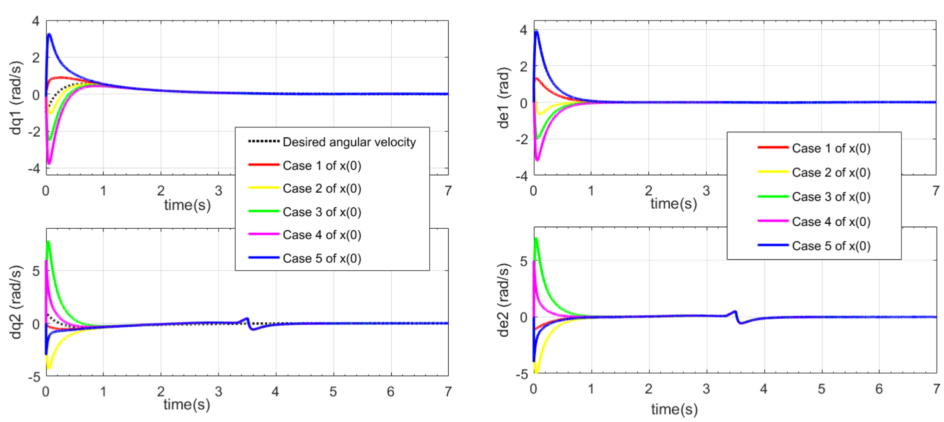

(a) Angular velocity tracking trajectory (b) Angular velocity tracking error trajectory

Figure 6 Angular velocity tracking trajectory and angular velocity tracking error trajectory of ARP and PRP in APDL-SM with five cases of initial states.

The angular velocity and its tracking error trajectory are exhibited in Figure 6(a) and Figure 6(b). The results prove the same property of fixed-time convergence for velocity tracking error.

However, it is obvious that all the response curves have a little hump corresponding to PRP and the tracking errors converges to zero with a extremely small deviation (within $\pm 5 \times 10^{-4}$). The reason is that NFTTSM controller is designed based on the assumption that the exact bound of lumped uncertaity $\Xi(x)$ is unknown in advance. To guarantee the stability and convergence of the tracking error, $\Xi(x)$ is chosen to be larger than the upper bound of the assumed fault magnitude. However, this approach limits its applications because a larger $\Xi(x)$ means a larger amplitude of switching in (4.11). Therefore, the difficulty of obtaining a precise distuebance upper bound function $\Xi(x)$ in advance in real application causes the NFTTSM controller has some deficiency in roustness.

5.3 Performance of RNFTTSM Control Scheme

On the basis of NFTTSM controller, we construct RNFTTSM control scheme to enhance the robustness by importing TDDO to estimate the unknown lumped uncertainties. The estimated uncertainties are then used to reconfigure the control system rapidly.

In this section, to better demonstrate the superiority of the RNFFTSM controller, NFTTSM and the adaptive SOFNTSM controller [[51]] are considered in simulations for the purpose of comparison.

The comparative simulations are conducted with the same initial conditions $x(0)^1 = [0.2, 2.1, 0, -0.1]^T$ in the presence of the same model uncertainties and external disturbances which share the same settings in Section 5.2.

As for controller parameters of RNFTTSM, they also share the same parameter settings as NFTTSM controller, which are $k_1 = 0.5, k_2 = 1, m = 5, n = 3, p = 1, q = 9, \beta_1 = \beta_2 = 8$.

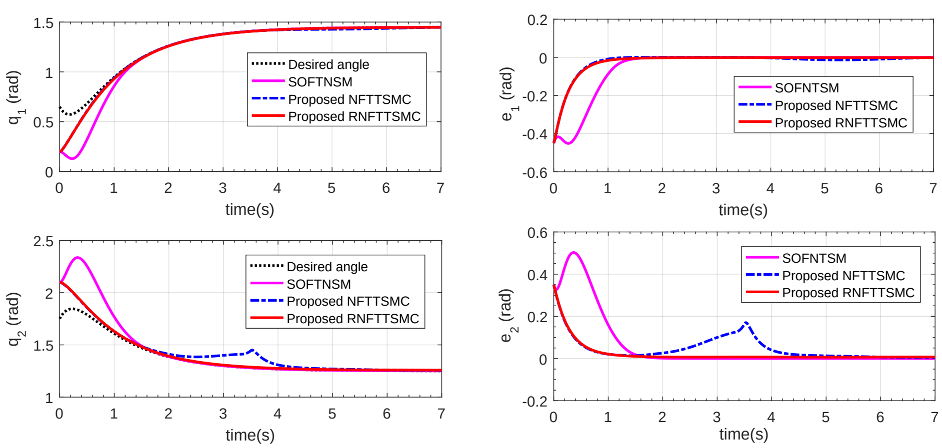

(a) Angle tracking trajectory (b) Angle tracking error

Figure 7 Angle tracking trajectory and tracking error trajectory of ARP and PRP in APDL-SM under three controllers.

The angle and angular velocity tracking performances of ARP and PRP under three controller are depicted in Figure 7 and Figure 8. All the response curves of the proposed RNFTTSM and NFTTSM controller are similar in the early stages, because the same basic control structure with identical parameters. It means that RNFTTSM also has the fixed time convergence performance.

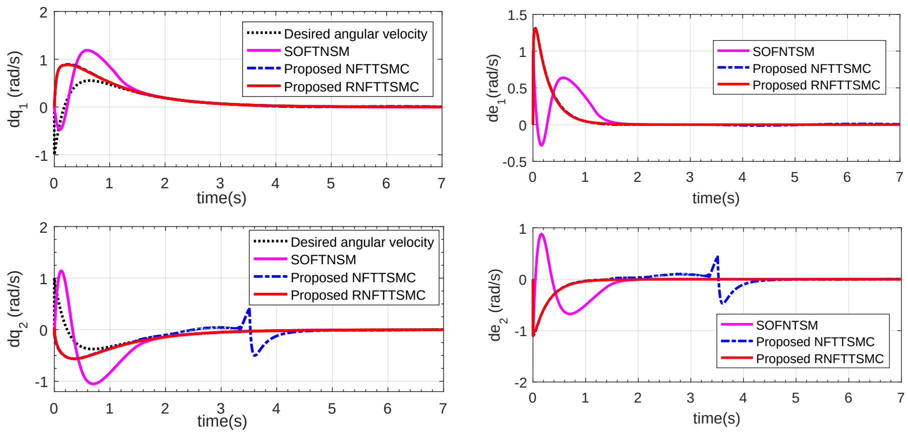

Angular velocity tracking error trajectory Angular velocity tracking trajectory

Figure 8 Angular velocity tracking trajectory and angular velocity tracking error trajectory of ARP and PRP in APDL-SM under three controllers.

However, after the system reaching a plateau, both RNFTTSM and SOFTNSM controller track the desired trajectories accurately and keep the tracking errors staying zero. The response curves of NFTTSM controller have a fluctuation at the tracking stage of PRP. These results show that RNFTTSM and SONFTSM have strong robustness. But Figure 7(b) and Figure 8(b) verify that RNFTTSM controller has a faster convergence rate.

Consequently, the simulation results reveal that the designed RNFTTSM control scheme can provide designable settling time (fixed-time convergence), faster global convergence rate, high-precision tracking and strong robustness.

6 Conclusion

To ensure a high-precision trajectory tracking control of APDL-SM under model uncertainty and lumped external disturbance, a novel RNFTTSM control scheme has been proposed and investigated in this paper. The proposed method mainly consists of the following three parts: (i) the FTTSS to provide the initial-state-independent convergence and designable convergence time in the sliding mode phase, (ii) the NFTTSM controller with the fixed time reaching law to achieve the fixed-time stability and a settling time estimate for the reaching phase, and (iii) the TDDO part to compensate the impact of model uncertainty and external disturbance on tracking performance and improve the robustness of the tracking system. The stability of the closed-loop control system is analyzed using Lyapunov method. Finally, the validity and superiorities of our proposed FTTSS, NFTTSM, and RNFTTSM control scheme are verified through simulation experiments.

References

[1] V. Eyring, I. S. Isaksen, T. Berntsen, W. J. Collins, J. J. Corbett, O. Endresen, R. G. Grainger, J. Moldanova, H. Schlager, D. S. Stevenson, Transport impacts on atmosphere and climate: Shipping, Atmospheric Environment 44 (37) (2010) 4735–4771.

[2] M. Sofiev, J. J. Winebrake, L. Johansson, E. W. Carr, M. Prank, J. Soares, J. Vira, R. Kouznetsov, J.-P. Jalkanen, J. J. Corbett, Cleaner fuels for ships provide public health benefits with climate tradeoffs, Nature Communications 9 (1) (2018) 406.

[3] D. Mueller, S. Uibel, M. Takemura, D. Klingelhoefer, D. A. Groneberg, Ships, ports and particulate air pollution-an analysis of recent studies, Journal of Occupational Medicine and Toxicology 6 (1) (2011) 31.

[4] T. I. IMO, Greenhouse gas study 2014, executive summary and final report, International Maritime Organization, London (2014) 57–58.

[5] T. Smith, J. Jalkanen, B. Anderson, J. Corbett, J. Faber, S. Hanayama, E. O'Keeffe, S. Parker, L. Johansson, L. Aldous, et al., Third IMO greenhouse gas study 2014, Int. Marit. Organ 327 (2014).

[6] M. Viana, P. Hammingh, A. Colette, X. Querol, B. Degraeuwe, I. de Vlieger, J. Van Aardenne, Impact of maritime transport emissions on coastal air quality in europe, Atmospheric Environment 90 (2014) 96–105.

[7] H. Liu, M. Fu, X. Jin, Y. Shang, D. Shindell, G. Faluvegi, C. Shindell, K. He, Health and climate impacts of ocean-going vessels in east asia, Nature Climate Change 6 (11) (2016) 1037.

[8] Q. Zhou, H. Li, P. Shi, Decentralized adaptive fuzzy tracking control for robot finger dynamics, IEEE Transactions on Fuzzy Systems 23 (3) (2014) 501–510.

[9] S. I. Han, J. M. Lee, Fuzzy echo state neural networks and funnel dynamic surface control for prescribed performance of a nonlinear dynamic system, IEEE Transactions on Industrial Electronics 61 (2) (2013) 1099–1112.

[10] H. R. Nohooji, Constrained neural adaptive pid control for robot manipulators, Journal of the Franklin Institute (2020).

[11] C. R. Kumar, K. Sudha, D. Pushpalatha, Design of prisoner's dilemma based fuzzy logic computed torque controller with lyapunov synthesis linguistic model for puma-560 robot manipulator, Journal of Intelligent & Fuzzy Systems 31 (1) (2016) 345–355.

[12] S. Z. A, M. R. S. B, Continuous fuzzy nonsingular terminal sliding mode control of flexible joints robot manipulators based on nonlinear finite time observer in the presence of matched and mismatched uncertainties, Journal of the Franklin Institute (2020).

[13] L. M. Capisani, A. Ferrara, Trajectory planning and second-order sliding mode motion/interaction control for robot manipulators in unknown environments, IEEE Transactions on Industrial Electronics 59 (8) (2011) 3189–3198.

[14] L. Derafa, A. Benallegue, L. Fridman, Super twisting control algorithm for the attitude tracking of a four rotors uav, Journal of the Franklin Institute 349 (2) (2012) 685–699.

[15] B. Xiao, S. Yin, O. Kaynak, Tracking control of robotic manipulators with uncertain kinematics and dynamics, IEEE Transactions on Industrial Electronics 63 (10) (2016) 6439–6449.

[16] Z. Cao, Y. Niu, Finite-time sliding mode control of markovian jump systems subject to actuator

nonlinearities and its application to wheeled mobile manipulator, Journal of the Franklin Institute 355 (16) (2018) 7865–7894.

[17] Q. Chen, L. Yu, Y. Nan, Finite-time tracking control for motor servo systems with unknown dead-zones, Journal of Systems Science and Complexity 26 (6) (2013) 940–956.

[18] Y. Wang, X. Wang, S. Zhao, L. Shen, Vector field based sliding mode control of curved path following for miniature unmanned aerial vehicles in winds, Journal of Systems Science and Complexity 31 (1) (2018) 302–324.

[19] W. Sun, Y. Wu, Modeling and finite-time tracking control for mobile manipulators with affine and holonomic constraints, Journal of Systems Science and Complexity 29 (3) (2016) 589–601.

[20] WANG, Jinran, LUO, Xiaoyuan, LI, Xiaolei, ZHU, Minggao, GUAN, Xinping, Sliding mode formation control of nonlinear multi-agent systems with local lipschitz continuous dynamics, Journal of Systems Science and Complexity (2019).

[21] LeipoLiu, ZhumuFu, XiaonaSong, An adaptive sliding mode control of delta operator systems with input nonlinearity containing unknown slope parameters, Journal of Systems Science and Complexity 30 (3) (2017) 535–549.

[22] M. Gan, Z. Qiao, Y. Li, Sliding mode control with perturbation estimation and hysteresis compensator based on bouc-wen model in tackling fast-varying sinusoidal position control of a piezoelectric actuator, Journal of Systems Science and Complexity 29 (2) (2016) 367–381.

[23] J. Chen, Y. Tian, P. Li, Q. Li, Z. Ren, Sliding-mode-control based robust guidance algorithm using only line-of-sight rate measurement, Journal of Systems Science and Complexity 29 (6) (2016) 1485–1504.

[24] Q. Chen, L. Tao, Y. Nan, Full-order sliding mode control for high-order nonlinear system based on extended state observer, Journal of Systems Science and Complexity 29 (4) (2016) 978–990.

[25] M. Zhihong, A. P. Paplinski, H. R. Wu, A robust mimo terminal sliding mode control scheme for rigid robotic manipulators, IEEE transactions on automatic control 39 (12) (1994) 2464–2469.

[26] K. Mei, S. Ding, X. Yang, L. Ma, Second-order sliding mode controller design with a larger domain of attraction, Journal of Systems Science and Complexity 33 (1) (2020) 61–73.

[27] Y. Guo, L. Yu, J. Xu, Robust finite-time trajectory tracking control of wheeled mobile robots with parametric uncertainties and disturbances, Journal of Systems Science and Complexity 32 (5) (2019) 1358–1374.

[28] S. S.-D. Xu, C.-C. Chen, Z.-L. Wu, Study of nonsingular fast terminal sliding-mode fault-tolerant control, IEEE Transactions on Industrial Electronics 62 (6) (2015) 3906–3913.

[29] X. Yu, M. Zhihong, Fast terminal sliding-mode control design for nonlinear dynamical systems, IEEE Transactions on Circuits and Systems I: Fundamental Theory and Applications 49 (2) (2002) 261–264.

[30] J. Zheng, H. Wang, Z. Man, J. Jin, M. Fu, Robust motion control of a linear motor positioner using fast nonsingular terminal sliding mode, IEEE/ASME Transactions on Mechatronics 20 (4) (2014) 1743–1752.

[31] A. Polyakov, Nonlinear feedback design for fixed-time stabilization of linear control systems, IEEE Transactions on Automatic Control 57 (8) (2011) 2106–2110.

[32] Z. Wang, J. Shan, Fixed-time consensus for uncertain multi-agent systems with actuator faults, Journal of the Franklin Institute 357 (2) (2020) 1199–1220.

[33] N. Wang, T. Zhang, Y. Yi, Q. Wang, Adaptive control of output feedback nonlinear systems with unmodeled dynamics and output constraint, Journal of the Franklin Institute 354 (13) (2017)

5176–5200.

[34] Y. H. Chen, X. Zhang, Adaptive robust approximate constraint-following control for mechanical systems, Journal of the Franklin Institute 347 (1) (2010) 69–86.

[35] B. Huo, Y. Xia, K. Lu, M. Fu, Adaptive fuzzy finite-time fault-tolerant attitude control of rigid spacecraft, Journal of the Franklin Institute 352 (10) (2015) 4225–4246.

[36] A. T. Vo, N. H. A. Nguyen, D. D. Pham, Integral sliding mode control for trajectory tracking control of robotic manipulators using an adaptive twisting algorithm, Journal of Science and Technology: Issue on Information and Communications Technology 17 (12.2) (2019) 42–47.

[37] G. R. Cho, P. H. Chang, S. H. Park, M. Jin, Robust tracking under nonlinear friction using time-delay control with internal model, IEEE Transactions on Control Systems Technology 17 (6) (2009) 1406–1414.

[38] M. Jin, Y. Jin, P. H. Chang, C. Choi, High-accuracy tracking control of robot manipulators using time delay estimation and terminal sliding mode, International Journal of Advanced Robotic Systems 8 (4) (2011) 33.

[39] K. Youcef-Toumi, O. Ito, A time delay controller for systems with unknown dynamics, in: 1988 American control conference, IEEE, 1988, pp. 904–913.

[40] M. Jin, J. Lee, P. H. Chang, C. Choi, Practical nonsingular terminal sliding-mode control of robot manipulators for high-accuracy tracking control, IEEE Transactions on Industrial Electronics 56 (9) (2009) 3593–3601.

[41] P. H. Chang, J. W. Jeong, Enhanced operational space formulation for multiple tasks by using time-delay estimation, IEEE Transactions on Robotics 28 (4) (2012) 773–786.

[42] M. Van, S. S. Ge, H. Ren, Finite time fault tolerant control for robot manipulators using time delay estimation and continuous nonsingular fast terminal sliding mode control, IEEE transactions on cybernetics 47 (7) (2016) 1681–1693.

[43] B. Brahmi, M. Saad, M. H. Rahman, A. Brahmi, Adaptive force and position control based on quasi-time delay estimation of exoskeleton robot for rehabilitation, IEEE Transactions on Control Systems Technology (2019).

[44] B. Siciliano, L. Sciavicco, L. Villani, G. Oriolo, Robotics: modelling, planning and control, Springer Science & Business Media, 2010.

[45] B. Brahmi, M. Saad, C. Ochoa-Luna, M. H. Rahman, A. Brahmi, Adaptive tracking control of an exoskeleton robot with uncertain dynamics based on estimated time-delay control, IEEE/ASME Transactions on Mechatronics 23 (2) (2018) 575–585.

[46] J. Ni, L. Liu, C. Liu, X. Hu, S. Li, Fast fixed-time nonsingular terminal sliding mode control and its application to chaos suppression in power system, IEEE Transactions on Circuits and Systems II: Express Briefs 64 (2) (2016) 151–155.

[47] Z. Zuo, Non-singular fixed-time terminal sliding mode control of non-linear systems, IET control theory & applications 9 (4) (2014) 545–552.

[48] P. H. Chang, J. W. Jeong, Enhanced operational space formulation for multiple tasks by using time-delay estimation, IEEE Transactions on Robotics 28 (4) (2012) 773–786.

[49] S. Roy, I. N. Kar, J. Lee, M. Jin, Adaptive-robust time-delay control for a class of uncertain euler–lagrange systems, IEEE Transactions on Industrial Electronics 64 (9) (2017) 7109–7119.

[50] J. Baek, W. Kwon, B. Kim, S. Han, A widely adaptive time-delayed control and its application to robot manipulators, IEEE Transactions on Industrial Electronics 66 (7) (2018) 5332–5342.

[51] S. Yi, J. Zhai, Adaptive second-order fast nonsingular terminal sliding mode control for robotic

manipulators, ISA Transactions 90 (2019) 41–51.